American Journal of Mechanics and Applications
2019; 7(3): 35-44
http://www.sciencepublishinggroup.com/j/ajma
doi: 10.11648/j.ajma.20190703.11
ISSN: 2376-6115 (Print); ISSN: 2376-6131 (Online)

Design and Finite Elements Analysis of a Hydraulic Excavator's Robot Arm System

Drissa Mohamed Malo[1, *], Erol Uzal[1], Sagnaba Soulama[2], Abdou-Salam Ganame[3]

[1]Mechanical Engineering Department, Faculty of Engineering, Istanbul University, Istanbul, Turkey

[2]Mechanical Engineering Department, Institute of Technology, Nazi Boni University, Bobo-Dioulasso, Burkina Faso

[3]Electrical Engineering Department, Institute of Technology, Nazi Boni University, Bobo-Dioulasso, Burkina Faso

Email address:

madrmo1993@gmail.com (D. M. Malo)

[*]Corresponding author

To cite this article:

Drissa Mohamed Malo, Erol Uzal, Sagnaba Soulama, Abdou-Salam Ganame. Design and Finite Elements Analysis of a Hydraulic Excavator's Robot Arm System. *American Journal of Mechanics and Applications.* Vol. 7, No. 3, 2019, pp. 35-44.
doi: 10.11648/j.ajma.20190703.11

Received: June 3, 2019; **Accepted**: July 15, 2019; **Published**: July 31, 2019

Abstract: Rapid growth of mining, construction and industrial activities is supported by automated high-performance machineries with sophisticated mechanism like hydraulic excavators. In this research paper, studies and researches have been carried out on the boom-arm-bucket robot system of a hydraulic excavator used especially on industrial, construction and mining sites. These studies provide general information about the technical specifications of this system. In order to improve the system's performances, finite elements stress analyses have been carried out. The studies begin with the design of the system using CAD (Computer Aided Design) software. Then a static force analysis of each component has been performed to determine the forces applied on them. The drawings were transferred to the finite element stress analysis software and all required steps for the analysis have been executed. The results obtained from the finite elements analysis revealed that the designed components were safe and subject to stress far below the assigned material's yield strength. However, the components were heavy and their weight could have been a disadvantage to their use. Design modifications have been performed in order lighten the components and at the same time to decrease their fabrication cost by decreasing the components thickness and changing the assigned material. These modifications also helped to improve their mobility.

Keywords: Excavator, Finite Element Stress Analysis, Modeling, Optimization, Robot Arm

1. Introduction

Rapid growth of the mining, construction and industrial activities is supported by automated high-performance machineries with sophisticated mechanism like hydraulic excavators. Hydraulic excavators are machines that can excavate various types of soil forcefully by using a powerful hydraulic system which provides lifting and digging force to the system [1]. They are heavy equipment that mainly consist of a boom, an arm or stick, a bucket and a cab on a rotating platform. The mobility of these machines is generally assured by either a system of two endless tracks (chain wheel system) or wheels. They are some of the most typical machines used in surface mining and construction sites for excavating and loading material.

Until the 19th century, heavy duty machines were drawn by human or animal power. Numerous and rapid scientific progresses have been made in the world since the 19th century. The advent of this era and the growing competitiveness allowed costumer companies and operators to gain access to more sophisticated products on the heavy equipment market [2]. Manufacturer increased safety, comfort, and reliability of their machines by using these new technologies. These numerous scientific advances also generated an exponential growth of some activities such as the construction, mining, forestry and industrial sectors.

In order to provide the construction or mining site with the best production rates and at the same time to ensure the company's profitability, it is it absolutely necessary to use the most suitable equipment for the excavation work [3]. This equipment needs to be optimized according to the

configuration and the needs of the site. The design and design modifications are very important stages that help to improve heavy equipment's effectiveness. The automation of an excavator needs a robotic system which is able to perform the planned digging work using its hydraulically operated mechanism known as the excavator's attachment. The robotic system of an excavator mainly consists of a boom, an arm and a bucket. These components form an articulated robot arm which performs the excavating operation. The mechanism is subject to intensive forces. In this study, excavator robot arm's components have been designed and their finite element stress analyses have been performed [4].

The articulated robot arm is one of the most important and also vulnerable parts of an excavator. The results of this research study would help to ensure the structural integrity of the boom, the arm, the bucket and other auxiliary components. It would help to avoid predictable accidents due to stresses above allowable limits for the system. Further, this study would also be a review on the finite elements stress analysis method which is the most widespread numerical procedure to solve a large class of engineering problems involving stress analysis [5]. It would enhance the knowledge of the reader about particularly the meshing, the applied external forces and loads, the material behavior simulation and the Von-Mises stress analysis with finite elements analysis software. It would also provide information about how to optimize this kind of mechanism in order to maintain its structural integrity.

The study has 3 main purposes. The first one is to design the excavator robot arm system's components using Computer Aided System (CAD) software. The second objective of the study is to make the finite elements stress analysis of the articulated robot arm's components by transferring the designed 3D parts to the finite element analysis software. All the steps of the process, from the meshing to the solution, have been followed. The third objective is to collect information and define parameters in order to optimize the system. All collected information has been analyzed.

2. Method

2.1. Material Characterization

In the mining sector, heavy equipment is used for heavy-duty tasks such as lifting, excavation, earthmoving, forestry, transportation, railroad operations. So, there are various types of heavy equipment and whose shapes, sizes and properties vary according to the configuration of the site where they will be working on and the tasks that they will be performing [6]. The excavator is one of the most common machines used in the mining and construction sectors. A conventional excavator usually has a long bucket arm attached to a pivoting cab that can rotate a full 360 degrees. We can classify excavators according to their locomotion mechanism. Consequently, there are two basic forms of excavator. On one hand there are some excavators using a system of two endless track system (Figure 1.) for their mobility. They are usually used on hilly areas where risks of sliding of the machines are on the verge. They are the most common ones because they have a better flotation, balance and better traction characteristics than the wheeled ones. On the other hand, there are also machines using conventional wheels which are generally used on plain ground operations. Wheeled excavators can generally travel up to 37 km/h. They can move quickly from a site to another one. They do not require additional transportation. They are practical for some applications like road maintenance which requires to travel while using a work tool [7].

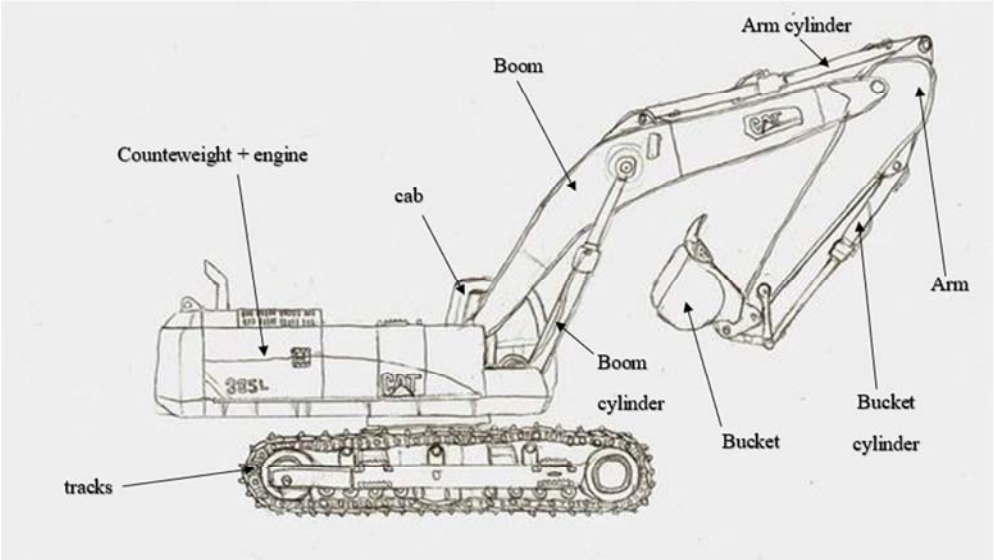

Figure 1. *Tracked excavator with its main components*[1].

1 https://soylentgreen44.deviantart.com/art/Excavator-outline-184280404

2.2. The Hydraulic System Components of a Hydraulic Excavator

As distinguished from other conventional vehicles like trucks or cars, the excavator does not use directly the energy generated by its motor's work. It uses hydraulic energy to perform all its tasks. This is what makes its hydraulic system, which turns the mechanical energy generated by the motor into hydraulic energy, one of its most important sections [8]. After being generated, the mechanical energy is transferred to the powerful hydraulic pump whose function is to keep the incompressible fluid in the tank under very high pressure. Then this hydraulic energy is transferred to a control valve which can be considered as the heart of the system. Its function is to apportion this energy to all the sections of the machine.

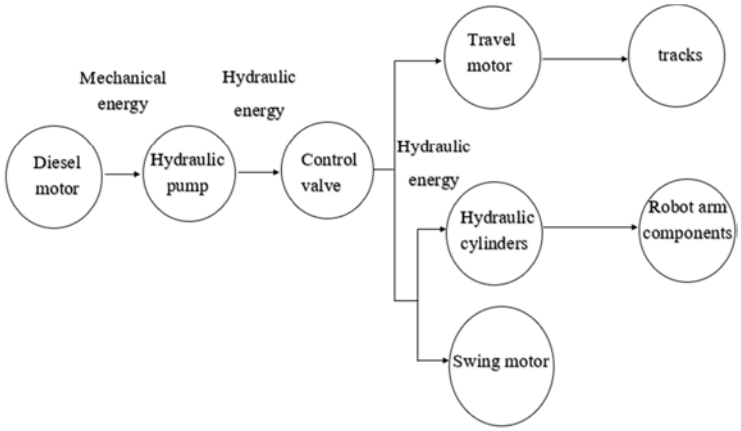

Figure 2. *Tracked excavator with its main components.*

2.3. The Main Components of the Robot Arm System

The boom bears the lifting and landing force. It is the component that connects the cab to the other attachments and is frequently the excavator's robot arm's biggest and longest operating component. It receives the energy from one or two boom cylinders depending on the machine's configuration. The arm is an extension of the boom which increases the maneuverability of the system. It is attached to the end of the boom. It provides the digging force needed to pull the bucket trough the ground. It receives the energy from one or two arm cylinders depending on the machine's configuration [9]. The bucket is located at the other end of the arm. It is the component which contains the earth and performs the excavation and digging operations. It owns long and sharp teeth whose role is to break through hard ground and rocks. It comes in numerous sizes and shapes depending on the application area [6]. It receives the energy from the bucket cylinder.

2.4. Design of the System's Component

The modelling of the components has been made in the SOLIDWORKS CAD-CAE software environment. The 2016 version has been used for that. The material used for the main components is the SAILMA 450 HI whose properties are in Table 1 and which is a material used in heavy equipment's design [10].

Table 1. *Properties of the SAILMA 450 HI material.*

Property	Value
Modulus of elasticity (E)	210000 $^{N}/_{mm^2}$
Poisson's ratio (μ)	0.3
Density (Rho)	900 $^{Kg}/_{m^3}$
Yield stress (σ_Y)	450MPa

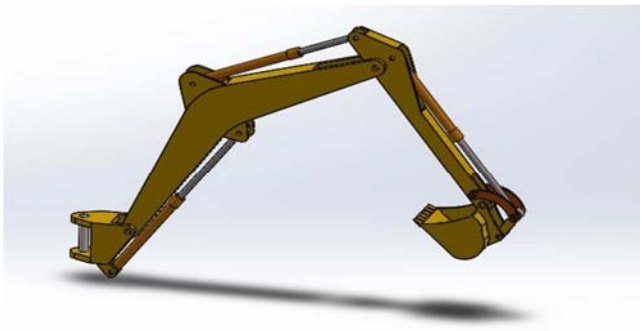

Figure 3. *Designed robot arm.*

2.5. The Maximum Breakout Configuration

The static force analysis is done considering the critical and highest stress conditions under which the system will be performing the excavation tasks [11]. The most critical configuration (figures 4&5) of this system is when the mechanism is producing the maximum breakout force because it generates the highest stress and is risky for the system's structural integrity. This maximum breakout force configuration is achieved when the arm is perpendicular to the arm cylinder. As shown on Figure 4, the arm axis is vertical, the arm cylinder is horizontal; consequently, there is an angle of 90° between them. The angle between the stabilizer connecting the bucket cylinder to the bucket and the horizontal axis is 85°. The angle between the cylinder and the horizontal axis is 37°. The static force analysis of this configuration will be carried out and will be used as a boundary condition for the finite element analysis in the following section of this work [12].

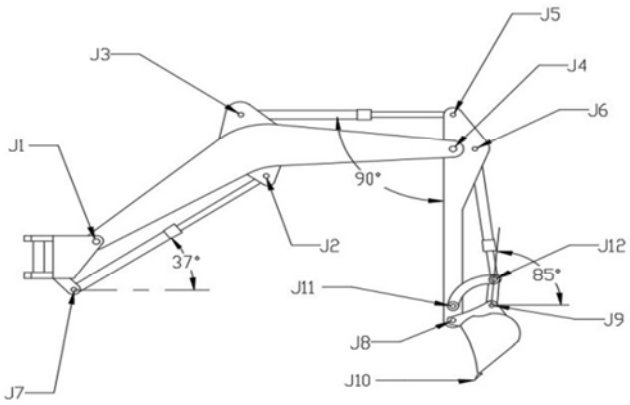

Figure 4. *Maximum breakout force configuration (with joints).*

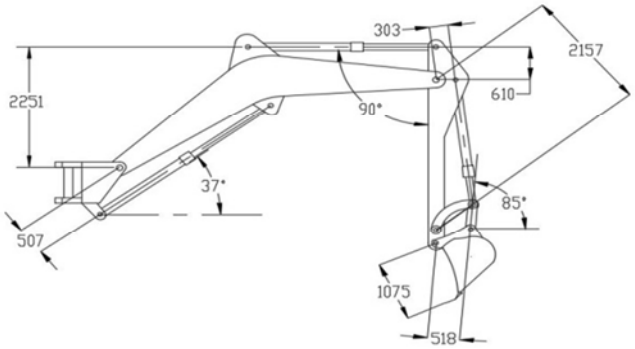

Figure 5. *Maximum breakout force configuration (with important dimensions).*

The hydraulic system, which commands our robot arm, provides a maximum breakout force of 30 kN at an angle of 25° between the bucket teeth blade and the ground. In the following section of our work, the free diagram of the arm, the boom and the bucket are defined and explained. Each component has been analyzed and forces coming on them have been calculated [13].

2.6. Static Force Analysis of the Bucket

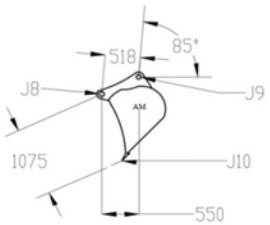

Figure 6. *The free body diagram, of the bucket.*

On Figure 6 bucket's J_9, J_{10} joints and their dimensions to the J_8 joint, are represented. The angle between the teeth's reaction force (30 kN) and the ground level is 25° at joint 10. The calculation of the static forces on joints has been performed by considering the 2 fundamental laws that are necessary for a system's static equilibrium:

The addition of all external forces must be equal to zero ($\Sigma F = 0$)

The addition of moments must be equal to zero ($\Sigma M = 0$).

The components of the reaction force F_{10} generated by the bucket teeth have been calculated by using equations (1), (2):

$$F_{10x} = F_{10} \cdot \cos\varphi \quad (1)$$

$$F_{10y} = F_{10} \cdot \sin\varphi \quad (2)$$

Where, φ is the angle between the teeth blade and the ground at maximum breakout force configuration (25°) and F_{10} is the maximum breakout force applied on joint J_{10}.

F_{10x} = 27.189 kN

F_{10y} = 12.678 kN

Now, the moment equilibrium law will be applied. By considering the summation of the moments about the joint J_8

$$F_{10} \cdot L_{10} - F_{gcb} \cdot L_{gcb} = F_9 \cdot L_9 \quad (3)$$

F_{10} is the force applied on the bucket tool tip when the bucket is at the maximum breakout force condition (30 kN).

L_{10}, is the distance between, J_{10} and, J_8 and perpendicular to F_{10} (1075 mm)

L_{gcb} is the horizontal distance between the bucket gravity center and J_8 (550 mm).

L_9 is the distance between J_8 and J_9 and perpendicular to F_{10} (518 mm).

F_{gcb} is the gravitational attraction applied by the earth on the bucket (9.8 kN)

F_9 is the force located on J_9 and it forms a β_9 angle of 85° with the horizontal plane. It will be calculated by using equation (3). Then, its components can be determined by using the (4) and (5) equations.

F_9 = 51.853 kN

$$F_{9x} = F_9 \cdot \cos\beta_9 \quad (4)$$

$$F_{9y} = F_9 \cdot \sin\beta_9 \quad (5)$$

F_{9x} = 4.519 kN

F_{9y} = 51.655 kN

From $\Sigma F = 0$; F_{8x} = 22.670 kN and F_{8y} = 38.977 kN

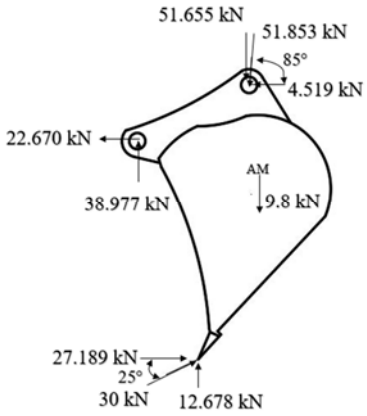

Figure 7. *Forces applied on the bucket.*

Table 2. *Values of forces applied on the bucket.*

Joints	horizontal forces F_x	vertical forces F_y
J8	-22.670 kN	38.977 kN
J_9	-4.519 kN	-51.655 kN
J_{10}	27.189 kN	12.678 kN

2.7. Static Force Analysis of the Arm

On figure 8 is represented the arm free body diagram. The Force F_{11} is the force applied on the tension bar (J_{11}-J_{12}) by the stabilizer (J_9-J_{12}) at an angle β 12a of 46°.

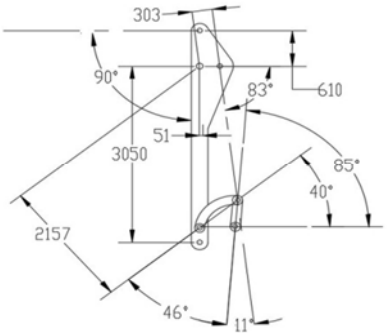

Figure 8. *The body diagram of the arm.*

$$F_{11} = F_9 \cdot \cos\beta_{12a} \quad (6)$$

F_{11} = 36.020 kN

The force F_6, which is applied by the bucket cylinder on the arm, forms an angle β_{12b} of 11° with the stabilizer's axis.

$$F_6 = F_9 \cdot \cos\beta_{12b} \quad (7)$$

F_6 = 50.900 kN

The components of the force F_{11} have been calculated by using the (8) and (9) equations. β_{11}, that is equal to 40°, is the angle formed by the tension bar's axis with the horizontal plane.

$$F_{11x} = F_{11} \cdot \cos\beta_{11} \quad (8)$$

$$F_{11y} = F_{11} \cdot \sin\beta_{11} \quad (9)$$

F_{11x}= 27.593 kN

F_{11y}= 23.153 kN

The components of the force F_6 have been determined by using the (10) and (11) equations. β_6, that is equal to 83°, is the angle formed by F_6 with the horizontal plane.

$$F_{6x} = F_6 \cdot \cos\beta_6 \quad (10)$$

$$F_{6y} = F_6 \cdot \sin\beta_6 \quad (11)$$

F_{6x} = 6.203 kN and F_{6y} = 50.521 kN

By applying the moment equilibrium about J_4;

$$F_5 \cdot L_5 = F_{8x} \cdot L_{8y} + F_{8y} \cdot L_{8x} + F_{11} \cdot L_{11} + F_6 \cdot L_6 - F_{gca} \cdot L_{gca} \quad (12)$$

F_5 is the force on the J_5 joint and can be determined by using the equation (12).

L_5 is the distance between the joints J_4 and J_5 in maximum breakout force condition and which is perpendicular to F_5 (610mm).

a. F_{8y} is the vertical component of the force applied on the joint J_8 (38.977 kN).
b. L_{8x} is the horizontal distance between J_8 and J_4 (0mm).
c. F_{gca} is the gravitational force on arm (14.210 kN).
d. L_{gca} is the horizontal distance between the gravity center of arm and J_4 (51 mm).
e. F_{8x} is the horizontal force component that acts on J_8 (22.670 kN).
f. L_{8y} is the vertical distance between the joint J_8 and the joint J_4 (3050 mm).
g. F_{11} is the force acting on tension bars due to the stabilizer (36.020 kN).
h. L_{11} is the distance between the joint J_4 and the joint J_{11} (2157 mm).
i. F_6 is the force applied on the arm by the bucket cylinder (50.900 kN).
j. L_6 is the distance between the joint J_4 and the joint J_6 and perpendicular to F_6 (303 mm).

F_5 = 264.814 kN

F_5 is horizontal. Consequently:

F_{5x}= 264.814 kN; F_{5y} = 0 kN

Considering $\Sigma F = 0$, F_4 that is the force applied on the joint J_4 has been determined.

F_{4x} = 308.874 kN,

F_{4y} = 34.697 kN

Table 3. *Values of forces applied on the arm.*

Joints	Horizontal forces F_x	Vertical Forces F_y
J_4	-308.874 kN	-34.697 kN
J_5	264.814 kN	0 kN
J_6	-6.203 kN	50.521 kN
J_8	22.670 kN	-38.977 kN
J_{11}	27.593 kN	23.153 kN

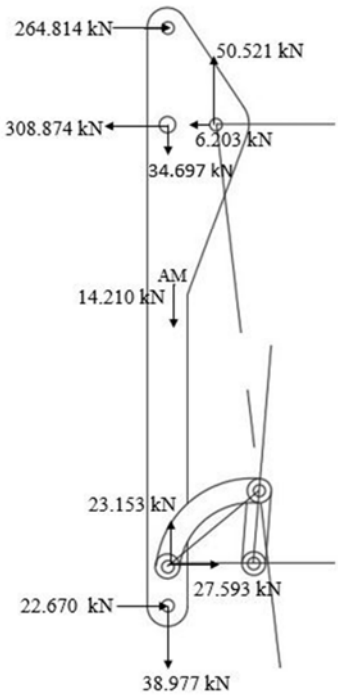

Figure 9. *Forces applied on the arm.*

2.8. Static Force Analysis of the Boom

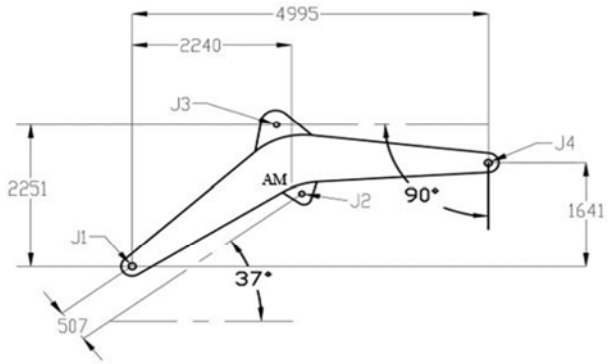

Figure 10. *Body diagram of the boom.*

The force F_3 is applied on the boom at J_3 by the arm cylinder and its value is equal to F_5's but they are opposite.

F_{3x}= 264.814 kN ve F_{3y} = 0 kN

By applying the moment equilibrium law about J1;

$$F_2 \cdot L_2 = F_{4y} \cdot L_{4x} + F_3 \cdot L_3 + F_{4x} \cdot L_{4y} - F_{gcbo} \cdot L_{gcbo} \quad (13)$$

force F_2 is applied on joint J_2 by the boom cylinder which forms a 37° angle with the horizontal plane.

a. L_2 is the distance between the joint J_2 and the joint J_1 and perpendicular to F_2 (507 mm).
b. F_{4x} is the horizontal component of F_4 and is equal to 308.874 kN
c. F_{4y} is the vertical component of F_4 and is equal to 34.697 kN.
d. L_{4x} and L_{4y} are the components of the distance between J_4 and J_1 and are respectively equal to 4995 mm and 1641 mm.
e. F_{gcbo}, is the gravitational attraction applied on the boom and is equal to 60.11 KN.
f. L_{gcbo} is the horizontal distance between the gravity center of the boom and J_1 and is equal to 2240 mm.
g. F_3 is the force applied on the joint J_3 (264.814 kN)
h. L_3 is the distance between the joint J_3 and the joint J_1 of (2251 mm)

F_2 = 252.311 kN

By using the (15) and (14) equations, the components of the force F_2 have been determined.

$$F_{2x} = F_2 \cdot \cos\beta_2 \quad (14)$$

$$F_{2y} = F_2 \cdot \sin\beta_2 \quad (15)$$

F_{2x}= 201.505 kN and F_{2y} = 151.845 kN

Considering ΣF = 0, forces applied on the joint J_1 have been calculated.

F_{1x}= 157.445 kN and F_{1y} = 117.148 kN

Table 4. *Values of forces applied on the boom.*

Joints	Horizontal forces F_x	Vertical Forces F_y
J_1	157.445 kN	117.148 kN
J_2	-201.505 kN	-151.845 kN
J_3	-264.814 kN	0 kN
J_4	308.874 kN	34.697 kN

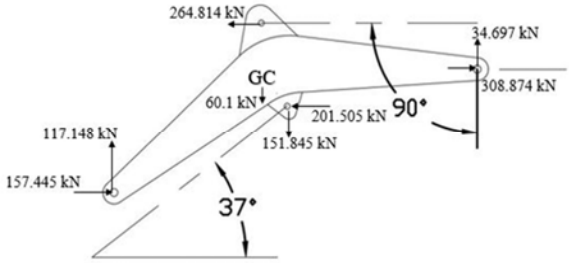

Figure 11. *Forces applied on the boom.*

2.9. Finite Elements Analysis

In many engineering problems, it is impossible to find an analytical solution by using the classic calculation methods. The finite elements method is a numerical procedure that is used to obtain the solution of some engineering problems involving stress analysis, heat transfer and fluid flow and which cannot be solved analytically. The finite elements method generally consists of 3 main phases which are necessary to solve the problem. These steps are divided into numerous other steps [5]. They are the preprocessing phase, the solution phase and the postprocessing phase. The following equations have been used for the preprocessing step:

The average stress on a section is:

$$\sigma = \frac{F}{A} \quad (16)$$

where F is the force applied to the element and A the section area

The average strain is determined by:

$$\varepsilon = \frac{\Delta_L}{L} \quad (17)$$

where Δ_L is the length variation and L is the length.

Over the elastic area the Hook's Law which is

$$\sigma = E\varepsilon \quad (18)$$

where E is the modulus of elasticity. Equations (16), (17) and (18) lead to:

$$F = \sigma A = E\varepsilon A = \left(\frac{EA}{L}\right)\Delta_L \quad (19)$$

$$F = keq\Delta_L \quad (20)$$

where keq is the equivalent stiffness of the element and F is the force applied on the element.

3. Results and Discussions

For each component studied in this document, finite elements analyses have been carried out in order to determine whether the system's structural integrity could resist to the intense forces work conditions [14]. The results provided by the software revealed that the calculated deformation and stress are largely below the SAILMA 450 HI materials yield strength. Consequently, the components design is safe.

However, the fact that the calculated stress and

deformation are low and far from the yield strength is a big advantage that provides a big optimization margin [15]. Indeed, it is necessary to provide the equipment not only with the maximum reliability, but also with the minimum weight and cost. Since the analyzed stresses are far below the SAILMA 450 HI's yield strength, the components have been redesigned with another material [16]. The structural steel has been selected for the substitution because it is cheaper, lighter and its yield strength is quite good. Its properties are in table 5.

Table 5. *Properties of the structural steel.*

Property	Value
Modulus of elasticity (E)	200000 $^{N}/_{mm^2}$
Poisson's ratio (μ)	0.3
Density (Rho)	7850$^{Kg}/_{m^3}$
Yield stress (σ_Y)	250MPa

In this optimization process, there are mainly a set of two variables. On one hand, we have the reliability, which is characterized by the stress. It is necessary to maintain the stress, whom the system is subject to, below the structural steel's yield strength. In order to maintain the structural integrity of the system, a safety stress margin of 75 MPa is considered for each component [17]. Moreover, it has been taken into consideration that the displacements of the bucket, arm, and boom should not be more than 4mm, 7mm and 4mm respectively. Let be a_i and U_i these variables. There are inequality constraints: $a_i \leq 175\,MPa;\ U_{bucket} \leq 4mm;\ U_{arm} \leq 7mm;\ U_{boom} \leq 4mm$.

On the other hand, the cost is a function of the weight. The lighter the system will be, the lower the cost will be. In order to lighten the system, thickness reductions have been performed.

3.1. Design Modification on the Bucket

Two main design modifications have been performed on the bucket. Firstly, the shell element´s thickness has been reduced from 40mm to 20mm. The teeth have been kept at the same size. Secondly the bucket's hook thickness has been reduced from 50mm to 25mm. This helped to reduce considerably the weight of the bucket and to increase its capacity at the same time since the thickness has been reduced from the inner areas. After the design modifications, the mass of the bucket fell from 1 t to 534 Kg. Its capacity increased from 0.5 to 0.55 m^3. The Von-Mises stress analysis (Figure 12) revealed that the maximum stress of the system increased from 38.636 MPa to 131.05 MPa. While the minimum value of stress increased from 0.20345 MPa to 0.49257 MPa. The maximum displacement increased from 0.77409 mm to 3.1825 mm which is quite negligible compared to the bucket's size. The optimization can be considered as safe [18].

Table 6. *Comparison of non-optimized and optimized bucket's analyses values.*

Non-optimized and optimized	Property	Maximum value	Minimum value
Non-optimized bucket	Von-Mises stress	38.636 MPa	0.20345 MPa
	Total deformation	0.77409 mm	0
	Mass	1 t	
	Capacity	0.5 m^3	
Optimized bucket	Von-Mises stress	131.05 MPa	0.49257 MPa
	Total deformation	3.1825 mm	0
	Mass	534 Kg	
	Capacity	0.55 m^3	

3.2. Design Modification on the Arm

On the arm which is also a shell element, design modifications have been made. The arm's plates thickness was initially 53 mm and has been reduced to 30 mm and this allowed to get rid of almost 1/3 of the initial weight. The Von-Mises stress analysis (Figure 13) revealed that the maximum stress of the system increased from 72.157 MPa to 117.55 MPa. The minimum value of the stress increased from 0.087185 MPa to 0.17538 MPa. The maximum displacement increased from 4.2636 mm to 6.517mm, which is quite negligible compared to the arm's size. The minimum displacement remains 0. The optimization is safe since the values of the maximum stress are below the defined value. The mass of the arm fell from 1.45 t to 944 Kg.

Table 7. *Comparison of non-optimized and optimized arm's analyses values.*

Non-optimized and optimized	Property	Maximum value	Minimum value
Non-optimized arm	Von-Mises stress	72.157 MPa	0.087185 MPa
	Total deformation	4.2636 mm	0
	Mass	1.45 t	
Optimized arm	Von-Mises stress	117.55 MPa	0.17538 MPa
	Total deformation	6.517mm	0
	Mass	944 Kg	

3.3. Design Modification on the Boom

The Boom is also a shell element like the bucket and the arm. The boom's plates initial thickness was 100 mm. Their thickness has been reduced to 50mm from the inner areas. Furthermore, the booms lower and upper hooks have also

been redesigned. Their initial thickness was 50mm and it has been reduced to 25 mm from the inner areas. The mass of the boom fell from 6.1t to 3,838t. The Von-Mises stress analysis (figure 14) revealed that the maximum stress of the system increased from 18.49 MPa to 40.481 MPa. While the minimum value of stress increased from 0.11447 MPa to 0.26057 MPa. The maximum displacement increased from 0.48933 mm to 3.1583 mm which is quite negligible compared to the arm's size. The optimization is safe since the values of the maximum stress are below the structural steel's yield strength.

Table 8. *Comparison of non-optimized and optimized boom's analyses values.*

Non-optimized and optimized	Property	Maximum value	Minimum value
Non-optimized boom	Von-Mises stress	18.49 MPa	0.11447 MPa
	Total deformation	0.48933 mm	0
	mass	6.1 t	
Optimized boom	Von-Mises stress	40.481 MPa	0.26057 MPa
	Total deformation	3.1583 mm	0
	mass	3,838 t	

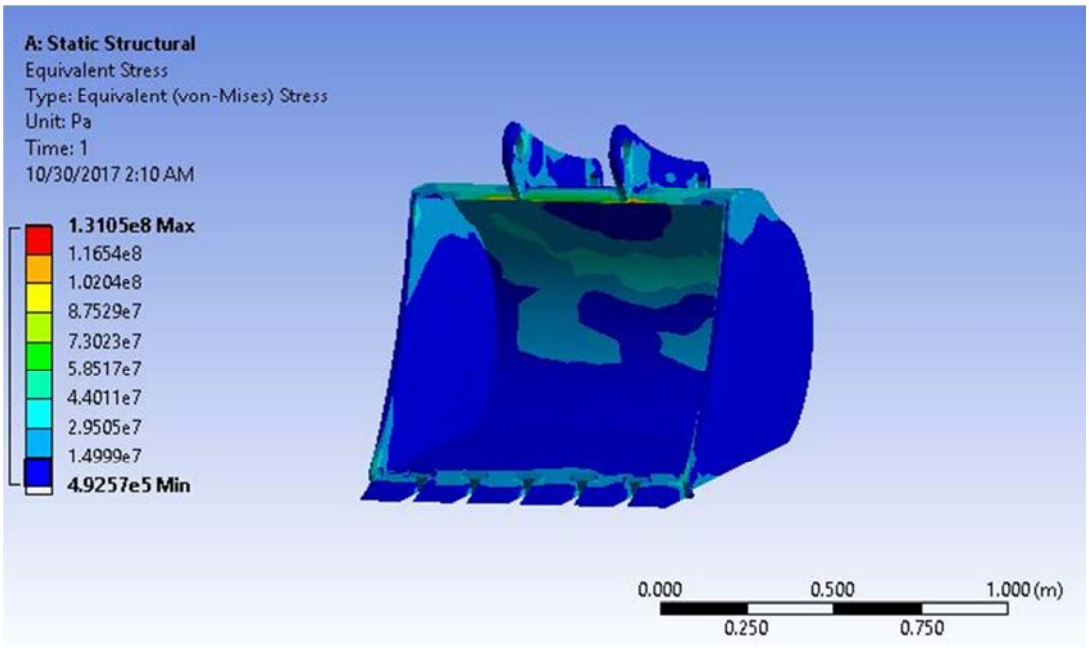

Figure 12. *The redesigned bucket's Von-Mises stress analysis.*

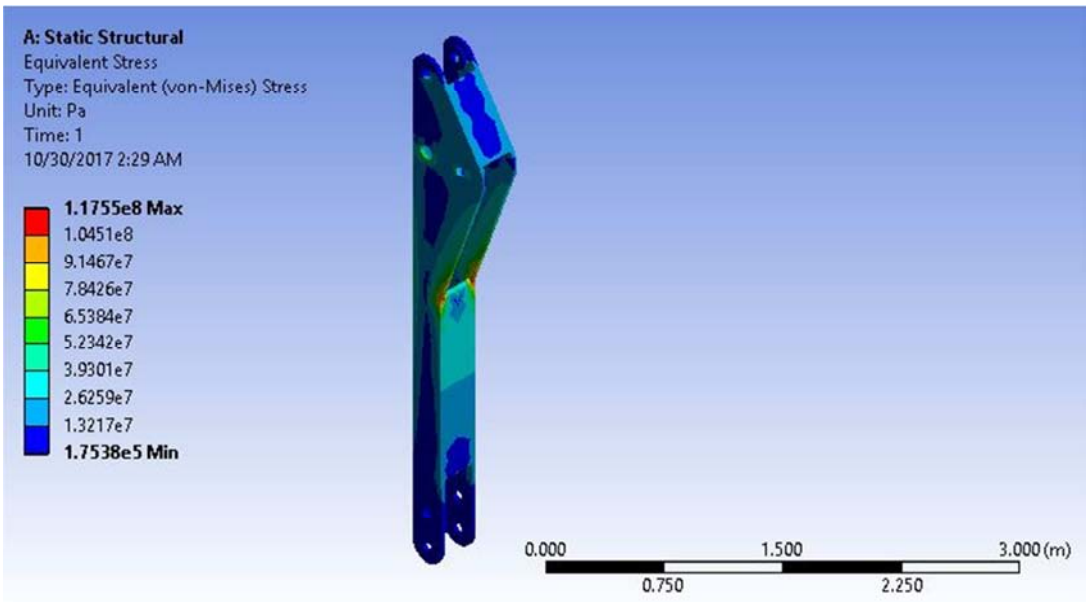

Figure 13. *The redesigned arm's Von-Mises stress analysis.*

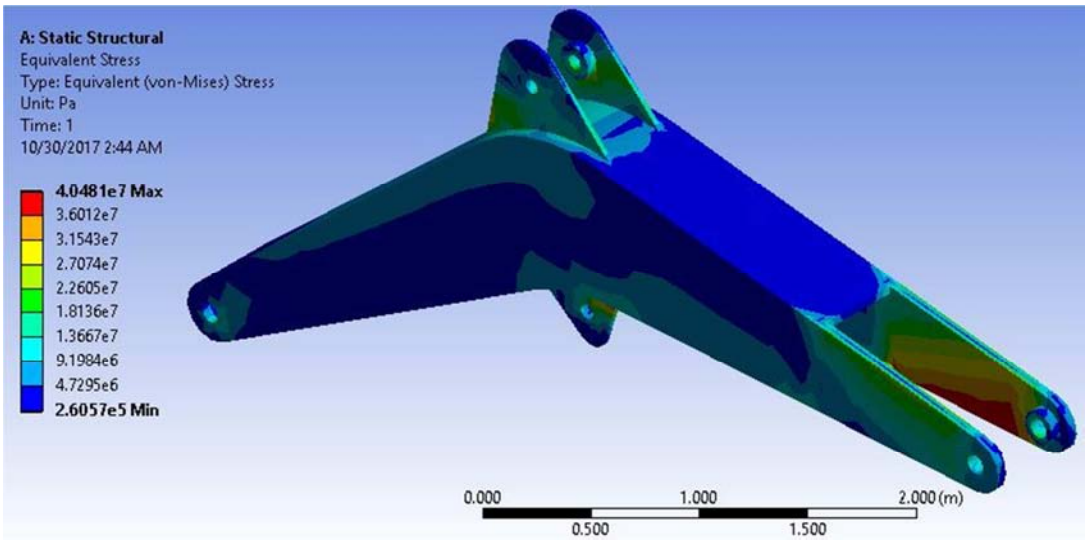

Figure 14. *The redesigned boom's Von-Mises stress analysis.*

The optimization helped to lighten the system by decreasing the components' thickness. This will provide many economic advantages:

A cheaper material has been used to redesigned the components and the quantity of material used to manufacture the components has decreased. Therefore, the cost will decrease.

The transportation of the attachments from the manufacturing factory to the assembly factory will be easier since the system's mass decreased.

The excavator´s hydraulic system will deal with a lighter system and this will help decrease the excavation cycle period as well as the lifting energy.

4. Conclusion

The purpose of this study was to design an excavator robot arm system, to perform its finite elements stress analysis, then optimize it on the basis of the finite element stress analyses' results. In order to model the system's components, a 3D CAD-CAE software has been used. The material used for the design has been chosen because of its favorable mechanical properties. Prior to the finite elements analysis, a static force analysis of the main components has been carried out. Forces applied on each component have been determined in the system's maximum breakout force configuration. In this configuration, the machines can provide their maximum breakout force. Consequently, it is the most critical and ideal configuration for finite elements static structural analysis.

Furthermore, the CAD models have been transferred to finite elements analysis software. The results obtained from the finite elements analysis revealed that the designed components are safe and subject to stress far below the assigned material's yield strength. However, the components were heavy and their weight could have been a disadvantage to their use. An optimization has been carried in order lighten the components and decrease their fabrication cost by reducing the component´s thickness and changing the material. After the optimization, the redesigned components have been retested and the obtained results revealed that the optimized components are reliable and subject to stress below the allowable limits.

Acknowledgements

The authors acknowledge Pr. Dr. Riza Güven the head of the Istanbul University mechanical engineering department for the services rendered.

References

[1] Afsar, J. (2012) Function of an Excavator. http://www.engineeringintro.com/all-about-construction-equipments/excavator-types-function-of-excavator.

[2] William, R. H. (2011) History of Construction Equipment. J Constr Eng Manag, 137, 720–723.

[3] Rodriguez, J. (2017) Must-Have Earth Moving Construction Heavy Equipment. https://www.thebalance.com/must-have-earth-moving-construction-heavy-equipment-844586.

[4] Mohamed, S. D. and Desai, H. (2014) Basic Concepts of Finite Element Analysis and its Applications in Dentistry: An Overview. J Oral Hyg Health, 5, 1-5.

[5] Saeed, M. (2007) Finite element analysis, theory and application with ANSYS. 3rd ed. USA: Prentice Hall.

[6] Krishna, I. V. (2015) Types of excavator, https://fr.slideshare.net/ilavamsikrishna/excavators-by-ila.

[7] Ilias, N. and Kleopatra, P. A. (2016) Thematic Review of the Main Research on Construction Equipment over Recent Years. Periodica Polytechnica Architecture, 47, 110-118.

[8] Caiyuan, X. and Zhang, G. (2015) Modal Analysis on Working Equipment of Hydraulic Excavator. The Open Mechanical Engineering Journal, 9, 173-180.

[9] Sarode, R. B. and Sarawade, S. S. (2016) Structural Optimization of Excavator Bucket Link. IOSR Journal of Mechanical & Civil Engineering, 2320-334X, 10-16.

[10] Bhaveshkumar, P. P. and Prajapati, J. M. (2011) A Review on FEA and Optimization of Backhoe Attachment in Hydraulic Excavator. Int J Chem Eng Appl, 5, 505-511.

[11] Venkata, A. R. and Hari, B. U. (2017) Optimal Design and Analysis of Twin Shaft Shredder. International Journal of research and innovation, 5, 805-813.

[12] Babu, A. M. (2015) Static Force Analysis of Mini Hydraulic Backhoe Excavator and Evaluation of Bucket Capacity, Digging Force Calculations. Int J Eng Res Appl, 2248-9622, 25-32.

[13] Sarode, R. B. and Sarawade, S. S. (2017) Topology Optimization of Excavator Bucket Link. IOSR Journal of Mechanical & Civil Engineering, 2320-334X, 12-26.

[14] Gui, J. Z., Cai, Y. X., You, Y. M., et al. (2013) Finite element analysis of working device for hydraulic excavator. J Chem Pharm Res, 5 (12), 123-128.

[15] Bende, S. B. and Awate, N. P. (2013) Computer Aided Design of Excavator Arm: Fem Approach. https://pdfs.semanticscholar.org/02c2/44708f35b4b0c3afa9bc4146a8eed9d3a778. pdf.

[16] Dhawalel, R. M. and Wagh, S. R. (2014) Finite Element Analysis of Components of Excavator Arm—A Review. *International Journal of Mechanical Engineering and Robotics Research*, 2, 340-346.

[17] Sekhar, B. S. and Venu, Y. (2014) Design optimization of excavator bucket using Finite Element Method. International Journal of Research and Innovation, 1, 76-84.

[18] Mitrev, R., Gruychev, R. and Pobegailo, P. (2011) CAD/CAE Investigation of a Large Hydraulic Mining Excavator. Machine Design, 1, 17-22.